AIAA 96-2517-CP

TWIN TAIL/DELTA WING CONFIGURATION BUFFET DUE TO UNSTEADY VORTEX BREAKDOWN FLOW

Osama A. Kandil, Essam F. Sheta and Steven J. Massey

Aerospace Engineering Department
Old Dominion University
Norfolk, VA 23529

The 14th AIAA Applied Aerodynamics Conference
New Orleans, LA-June 18-20, 1996

COMPUTATION AND VALIDATION OF FLUID/ STRUCTURE TWIN TAIL BUFFET RESPONSE

Osama A. Kandil and Essam F. Sheta
Aerospace Engineering Department
Old Dominion University, Norfolk, VA 23529, USA

C. H. Liu
Aerodynamics Methods and Acoustics Branch
NASA Langley Research Center, Hampton, VA 23665, USA

EUROMECH COLLOQUIUM 349
STRUCTURE FLUID INTERACTION IN AERONAUTICS
Institute Für Aeroelastik, Göttingen, Germany
September 16-18, 1996

COMPUTATION AND VALIDATION OF FLUID/STRUCTURE TWIN TAIL BUFFET RESPONSE

Osama A. Kandil[1] and Essam F. Sheta[2]
Aerospace Engineering Department
Old Dominion University, Norfolk, VA 23529, USA
and
C. H. Liu[3]
Aerodynamics Methods and Acoustics Branch
NASA Langley Research Center, Hampton, VA 23665, USA

ABSTRACT

The buffet response of the flexible twin-tail/delta wing configuration-a multidisciplinary problem is solved using three sets of equations on a multi-block grid structure. The first set is the unsteady, compressible, full Navier-Stokes equations which are used for obtaining the flow-filed vector and the aerodynamic loads on the twin tails. The second set is the coupled aeroelastic equations which are used for obtaining the bending and torsional deflections of the twin tails. The third set is the grid-displacement equations which are used for updating the grid coordinates due to the tail deflections. The computational model is similar to the one used by Washburn et. al. which consists of a delta wing of aspect ratio one and twin tails with taper ratios of 0.23. The vertex of the twin tails are located at the wing trailing edge. The configuration is pitched at 30° angle of attack and the freestream Mach number and Reynolds number are 0.3 and 1.25 million, respectively. With the twin tails fixed as rigid surfaces, the problem is solved for the initial flow conditions. Next, the problem is solved for the twin tail response for uncoupled bending and torsional vibrations due to the unsteady loads produced by the vortex breakdown flow of the leading-edge vortex cores. The configuration is investigated for three spanwise positions of the twin tails; inboard, midspan and outboard locations. The computational results are validated and are in very good agreement with the experimental data of Washburn, et. al.

INTRODUCTION

The ability of modern fighter aircraft to fly and maneuver at high angles of attack and at high loading conditions is of prime importance. This capability is achieved, for example in the F/A-18 fighter, through the combination of the leading-edge extension (LEX) with a delta wing and the use of vertical tails. The LEX maintains lift at high angles of attack by generating a pair of vortices that trail aft over the top of the aircraft. The vortex entrains air over the vertical tails to maintain stability of the aircraft. At some flight conditions, the vortices emanating from the highly-swept LEX of the delta wing breakdown before reaching the vertical tails which get bathed in a wake of unsteady highly-turbulent, swirling flow. The vortex-breakdown flow produces unsteady, unbalanced loads on the vertical tails which in turn produce severe buffet on the tails and has led to their premature fatigue failure.

Experimental investigation of the vertical tail buffet of the F/A-18 models have been conducted by several investigators such as Sellers, et al. (Ref 1), Erickson, et al. (Ref 2), Wentz (Ref 3) and Lee and Brown (Ref 4). These experiments showed that the vortex produced by the LEX of the wing breaks down ahead of the vertical tails at angles of attack of 25° and higher and the breakdown flow produced unsteady loads on the vertical tails. Cole, Moss and Doggett (Ref 5) tested a rigid, 1/6 size, full-span model of an F-18 airplane that was fitted with flexible vertical tails of two different stiffness.

[1]Professor, Eminent Scholar and Dept. Chair.
[2]Ph.D. Graduate Research Assistant.
[3]Senior Scientist.

Vertical-tail buffet response results were obtained over the range of angle of attack from $-10°$ to $+40°$, and over the range of Mach numbers from 0.3 to 0.95. Their results indicated that the buffet response occurs in the first bending mode, increases with increasing dynamic pressure and is larger at $M = 0.3$ than that at a higher Mach number.

An extensive experimental investigation has been conducted to study vortex-tail interaction on a $76°$ sharp-edged delta wing with vertical twin-tail configuration by Washburn, Jenkins and Ferman (Ref 6). The vertical tails were placed at nine locations behind the wing. The experimental data showed that the aerodynamic loads are more sensitive to the chordwise tail location than its spanwise location. As the tails were moved laterally toward the vortex core, the buffeting response and excitation were reduced. Although the tail location did not affect the vortex core trajectories, it affected the location of vortex-core breakdown. Moreover, the investigation showed that the presence of a flexible tail can affect the unsteady pressures on the rigid tail on the opposite side of the model. In a recent study by Bean and Lee (Ref 7) tests were performed on a rigid 6% scale F/A-18 in a trisonic blowdown wind tunnel over a range of angle of attack and Mach number. The flight data was reduced to a non-dimensional buffet excitation parameter, for each primary mode. It was found that buffeting in the torsional mode occurred at a lower angle of attack and at larger levels compared to the fundamental bending mode.

Kandil, Kandil and Massey (Ref 8) presented the first successful computational simulation of the vertical tail buffet using a delta wing-single flexible vertical tail configuration. The tail was allowed to oscillate in bending modes. The flow conditions and wing angle of attack have been selected to produce an unsteady vortex-breakdown flow. Unsteady vortex breakdown of leading-edge vortex cores was captured, and unsteady pressure forces were obtained on the tail. These computational results are in full qualitative agreement with the experimental data of Washburn, Jenkins and Ferman (Ref 6). The total deflections and the frequencies of deflections and loads of the coupled bending-torsion case were found to be one order of magnitude higher than those of the bending case only. Also, it has been shown that the tail oscillations change the vortex breakdown locations and the unsteady aerodynamic loads on the wing and tail.

Kandil, Massey and Sheta (Ref 9) studied the effects of coupling and uncoupling the bending and torsional modes for a long computational time, and the flow Reynolds number on the buffet response.

In this paper, we consider the buffet response of the F-117 flexible twin tail configuration similar to the one used by Washburn, et. al. (Ref 6). A multi-block grid is used to solve the problem for three spanwise locations of the twin tails; inboard, midspan and outboard locations. The aeroelastic equations are used to solve for uncoupled bending-torsion responses. The computational results are compared with the experimental data of Washburn, et. al. They are in very good agreement with these data.

HIGHLIGHTS OF THE FORMULATION AND COMPUTATIONAL SCHEMES

The formulation of the problem consists of three sets of governing equations along with certain initial and boundary conditions. The first set is the unsteady, compressible, full Navier-Stokes equations. The second set consists of the aeroelastic equations for bending and torsional modes. The third set consists of equations for deforming the grid according to the tail deflections. Details of the problem formulation are given in (Ref 10) by the first two authors. The first step is to solve for the fluid flow problem using vortex-breakdown conditions and keeping the twin tails rigid. Navier-Stokes equations are solved using the implicit, flux-difference splitting finite-volume scheme. The grid speed $\frac{\partial \xi^m}{\partial t}$ is set equal to zero in this step. This step provides the flow field solution along with the pressure difference across the tails. The pressure difference is used to generate the normal force and twisting moment per unit length of each tail. Next, the aeroelastic equations are used to obtain the bending and torsion deflections of each tail, $w_{i,j,k}$ and $\theta_{i,j,k}$. The grid displacement equations are then used to compute the new grid coordinates. The metric coefficient of the coordinate Jacobian matrix are updated as well as

the grid speed, $\frac{\partial \xi^m}{\partial t}$. At each time step, the computational cycle consisting of the Navier-Stokes solver, the aeroelastic equations solver, and the grid displacement solver is repeated.

COMPUTATIONAL APPLICATIONS AND DISCUSSION

Twin Tail-Delta Wing Configuration:

The twin tail-delta wing configuration consists of a 76°-swept back, sharp-edged delta wing (aspect ratio of one) and dynamically scaled flexible twin tails similar to those used by Washburn, et. al. (Ref 6). The vertical tails are oriented normal to the upper surface of the delta wing and have a centerline sweep of 53.5°. Each tail is made of a single Aluminum spar and Balsa wood covering. The Aluminum spar has a taper ratio of 0.3 and a constant thickness of 0.001736. The chord length at the root is 0.03889 and at the tip is 0.011667, with a span length of 0.2223. The Aluminum spar is constructed from 6061-T6 alloy with density, ρ, modulii of elasticity and rigidity, E and G of 2693 kg/m^3, $6.896X10^{10}\ N/m^2$ and $2.5925X10^{10}\ N/m^2$; respectively. The Balsa wood covering has a taper ratio of 0.23 and aspect ratio of 1.4. The chord length at the root is 0.2527 and at the tip is 0.058, with a span length of 0.2223. The Balsa thickness decreases gradually from 0.0211 at the tail root to 0.0111 at the tail midspan and then constant thickness of 0.0111 is maintained to the tail tip. The tail cross section is a semi-diamond shape with bevel angle of 20°. The Balsa density, modulii of elasticity and rigidity, E and G, are 179.7 kg/m^3, $6.896X10^8\ N/m^2$ and $2.5925X10^8\ N/m^2$; respectively. The tails are assumed to be magnetically suspended and the leading edge of the tail root is positioned at $x/c = 1.0$, measured from the wing apex. The configuration is pitched at an angle of attack of 30° and the freestream Mach number and Reynolds number are 0.3 and 1.25 x 10^6; respectively.

A multi-block grid consisting of 4 blocks is used for the solution of the problem. The first block is a O-H grid for the wing and upstream region, with 101X50X54 grid points in the wrap around, normal and axial directions, respectively. The second block is a H-H grid for the inboard region of the twin tails, with 23X50X13 grid points in the wrap around, normal and axial directions, respectively. The third block is a H-H grid for the outboard region of the twin tails, with 79X50X13 grid points in the wrap around, normal and axial directions, respectively. The fourth block is a O-H grid for the downstream region of the twin tails, with 101X50X25 grid points in the wrap around, normal and axial directions, respectively. Figure 1 shows the grid topology and a blow-up of the twin tail-delta wing configuration.

The configuration is investigated for three spanwise positions of the twin tails; the inboard location, the midspan location and the outboard location corresponding to a separation distance between the twin tails of 33%, 56% and 78% of the wing span; respectively.

Inboard Location of Twin Tails (33 % wing span):

The spanwise distance between the two tails is 33 % of the wing span. Figure 2 shows three-dimensional and front views for the initial conditions with the surface total pressure contours and the streamlines of the vortex cores. The initial conditions are obtained after 10,000 time steps, $\Delta t = 0.001$, with the twin tails kept rigid. It is observed that the vortex cores experience symmetric breakdown on the wing at about the 75% chordstation. Downstream of the wing, they are totally outside of the space between the twin tails. Smaller size vortex cores appear under the vortex breakdown flows and at the lower edges of the twin tails. These results exactly match Washburn observations. Figure 3 shows the results for the twin tails undergoing uncoupled bending-torsion responses after 9,600 time steps from the initial conditions. It is observed that the breakdown shapes and locations are affected by the twin tail oscillations. The vortex breakdown is now asymmetric, and the vortex breakdown flows are still outside of the space between the twin tails. These results conclusively show the upstream as well as the spanwise effects of the twin tail oscillations on the vortex breakdown flows.

Figures 4-6, show the distribution of deflection and load responses along the left and right tails every 2000 time steps, the history of deflection and load responses versus time and the total structural deflections and root bending moment for the left and right tails. It is observed that the bending and torsion responses are in their first and second mode shapes. The frequencies of the bending deflections are less than one-half those of the torsion deflections. The normal forces are out of phase of the bending deflections while the torsion moments are in phase with the torsion deflections. The total tail responses are in first, second and third mode shapes. Periodic responses have not been reached within the computational time covered (20,000 time steps = 10 dimensionless time units).

Midspan Location of Twin Tails (56% wing span):

The results of this case are presented in Figs. 7-10. Figure 7 shows that the tails cut through the vortex breakdown of the leading-edge vortex cores, which are also asymmetric. Figure 8 shows that the bending deflections are lower than those of the inboard case while the torsional deflections are substantially lower than those of the inboard case. Moreover, the bending and torsion deflections have a single sign for the left and right tails (all are positive or all are negative). Figure 9 shows that both bending and torsion deflections are out of phase of the normal force and twisting moment loads. The total deflections of Fig. 10 shows the same trend. The root bending moments of Fig. 10 are also lower than those of the inboard case.

Outboard Location of Twin Tails (78% wing span):

Figures 11-14 show the results of this case. Figure 11 shows that the space between the twin tails include larger portion of the vortex breakdown flow of the leading-edge vortex cores, than that of the midspan case. The vortex breakdown flow is also asymmetric. The vortical flow on the lower outside surfaces of the twin tails is larger than any of the above two cases. Figures 12-14 show that the bending and torsion deflections are lower than those of the midspan case. They also show that both bending and torsion deflections are out of phase of the bending and torsional loads. The frequencies of the bending deflections are still smaller than those of the torsion deflections. All these observations are in very good agreement with those of Washburn, et. al. (Ref 6).

Table (1) shows a comparison of the mean root bending moment for flexible twin tails and the lift coefficient with rigid twin tails of the computed results with those of Washburn, et. al. (Ref 6).

Parameter	Position	FTNS3D	WASHBURN
Mean Root Bending Moment With Flexible Tails	Inboard	$5.62X10^{-5}$	$7.43X10^{-5}$
	Midspan	$4.22X10^{-5}$	$6.05X10^{-5}$
	Outboard	$3.62X10^{-5}$	$5.70X10^{-5}$
Lift Coefficient With Rigid Tails	Inboard	1.0423	1.17
	Midspan	1.0515	1.12
	Outboard	1.0674	1.17

Table (1) Validation of FTNS3D computational results with Washburn, et. al. experimental results.

CONCLUDING REMARKS

The computational results of the FTNS3D code of the present paper and the experimental data of Washburn, et. al. are in very good agreement for the Washburn, et. al. configuration at 30° angle of attack and the three spanwise locations of the twin tails. It is concluded that the inboard location

of the twin tails produces the largest bending-torsion loads, deflections, frequencies and root bending moments when compared with the midspan and outboard locations. The outboard location produce the least of these responses. When the twin tails cut through the vortex breakdown flow, they produce less responses due to the compensating damping effect produced by the left and right parts of the vortex breakdown flow on each tail.

ACKNOWLEDGMENT

For the first two authors, this research work is supported under Grants No. NAG-1-994 by the NASA Langly Research Center. The authors would like to recognize the computational resources provided by the NAS facilities at Ames Research Center and the NASA Langley Research Center.

REFERENCES

1. Sellers, W. L. III, Meyers, J. F. and Hepner, T. E., "LDV Survey Over a Fighter Model at Moderate to High Angle of Attack," SAE Paper 88-1448, 1988.

2. Erickson, G. E., Hall, R. M., Banks, D. W., Del Frate, J. H., Shreiner, J. A., Hanley, R. J. and Pulley, C. T., "Experimental Investigation of the F/A-18 Vortex Flows at Subsonic Through Transonic Speeds," AIAA 89-2222, 1989.

3. Wentz, W. H., "Vortex-Fin Interaction on a Fighter Aircraft," AIAA 87-2474, AIAA Fifth Applied Aerodynamics Conference, Monterey, CA August 1987.

4. Lee, B. and Brown, D., "Wind Tunnel Studies of F/A-18 Tail Buffet," AIAA 90-1432, 1990.

5. Cole, S. R., Moss, S. W. and Dogget, R. V., Jr., "Some Buffet Response Characteristics of a Twin-Vertical-Tail Configuration," NASA TM-102749, October 1990.

6. Washburn, A. E., Jenkins, L. N. and Ferman, M. A., "Experimental Investigation of Vortex-Fin Interaction," AIAA 93-0050, AIAA 31st ASM, Reno, NV, January 1993.

7. Bean, D. E. and Lee, B. H. K., "Correlation of Wind Tunnel and Flight Test Data for F/A-18 Vertical Tail Buffet," AIAA 94-1800-CP, 1994

8. Kandil, O. A., Kandil, H. A. and Massey, S. J., "Simulation of Tail Buffet Using Delta Wing-Vertical Tail Configuration," AIAA 93-3688-CP, AIAA Atmospheric Flight Mechanics Conference, Monterery, CA August 1993, pp. 566-577.

9. Kandil, O. A., Massey, S. J. and Sheta, E. F., "Structural Dynamics/CFD Interaction for Computation of Vertical Tail Buffet," International Forum on Aeroelasticity and Structural Dynamics, Royal Aeronautical Society, Manchester, U.K., June 26-28, 1995. Also published in Royal Aeronautical Journal, August/September 1996, pp. 297-303.

10. Kandil, O. A., Sheta, E. F. and Massey, S. J., "Twin Tail/Delta Wing Configuration Buffet Due to Unsteady Vortex Breakdown Flow," AIAA 96-2517-CP, 14th AIAA Applied Aerodynamics Conference, New orleans, LA, June 18-20, 1996, pp. 1136-1150.

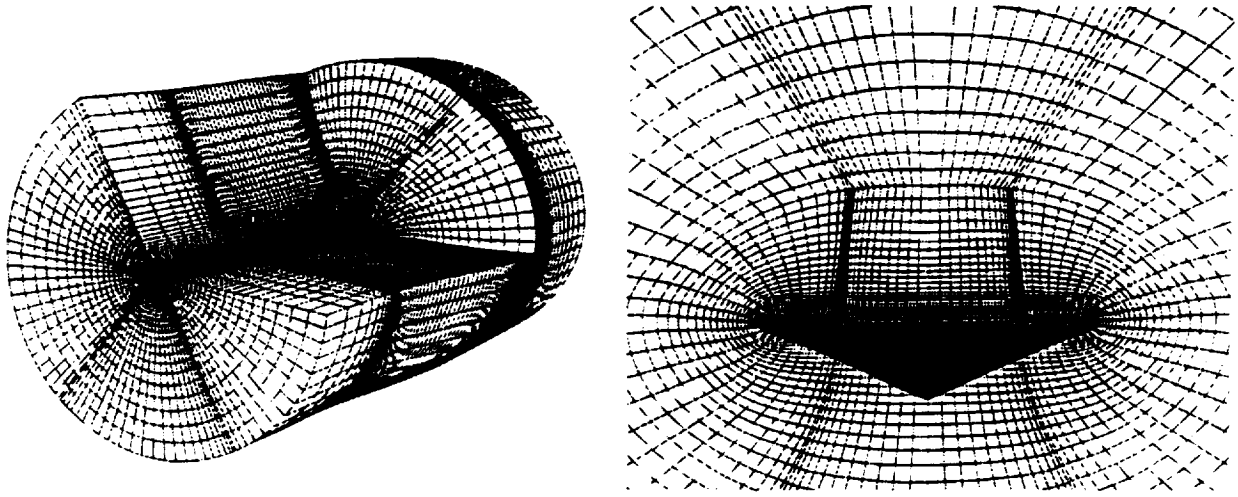

Figure 1: Three-dimensional grid topology and blow-up of the wing-twin tail configuration (Midspan position).

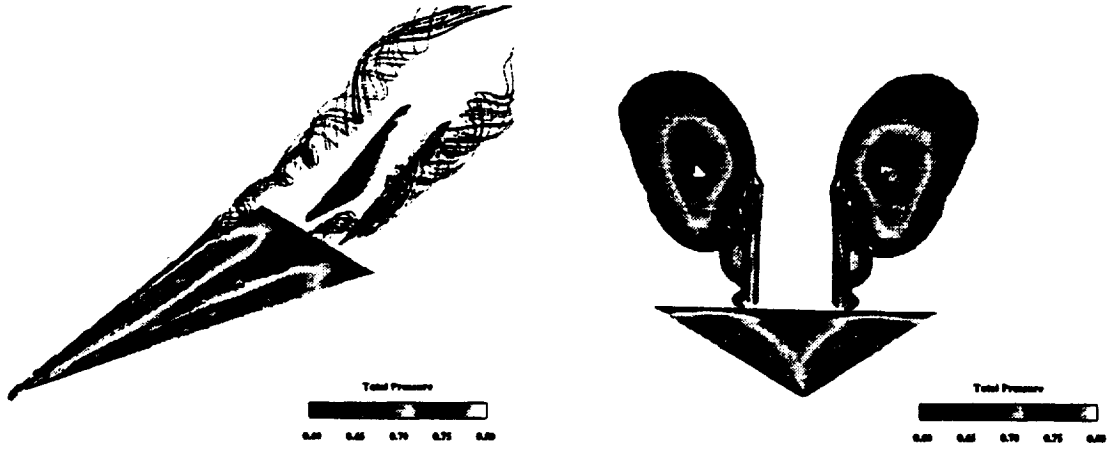

Figure 2: Three-dimensional and front views showing the total pressure on the surfaces, and the vortex-core streamlines. Initial conditions (Inboard position).

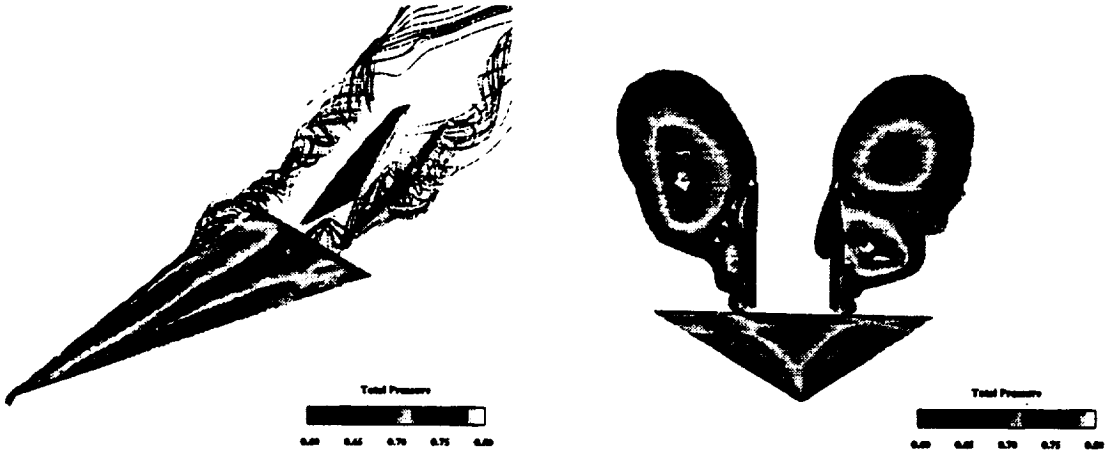

Figure 3: Three-dimensional and front views showing the total pressure on the surfaces, and the vortex-core streamlines. Uncoupled case after $it = 9,600$ (Inboard position).

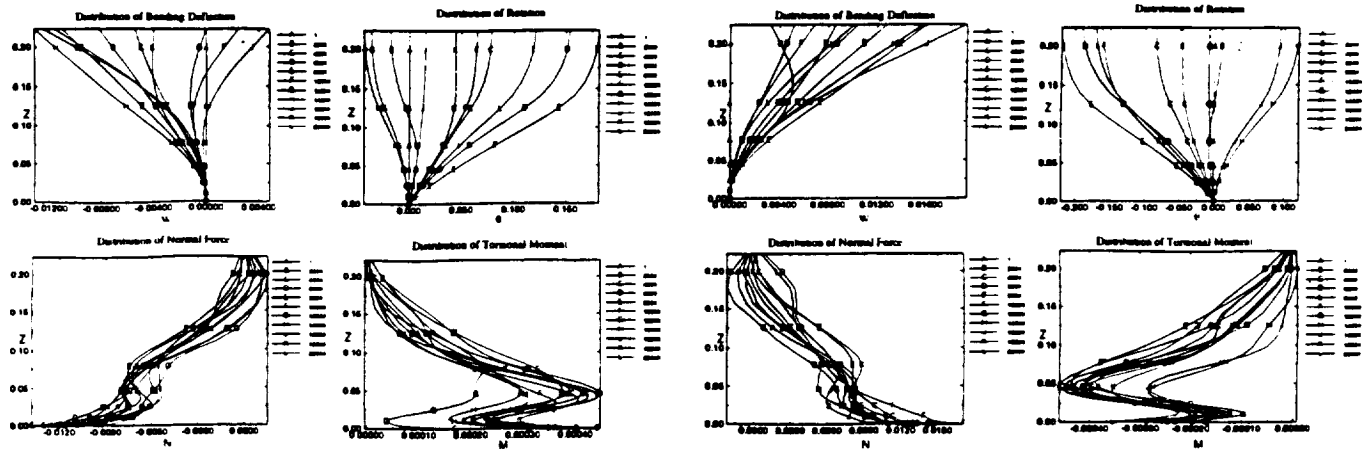

(a) Left tail (b) Right tail

Figure 4: Distribution of the deflection and load responses for an uncoupled bending-torsion case. $M_\infty = 0.3$, $\alpha = 30^o$, $R_e = 1.25x10^6$, (Inboard position).

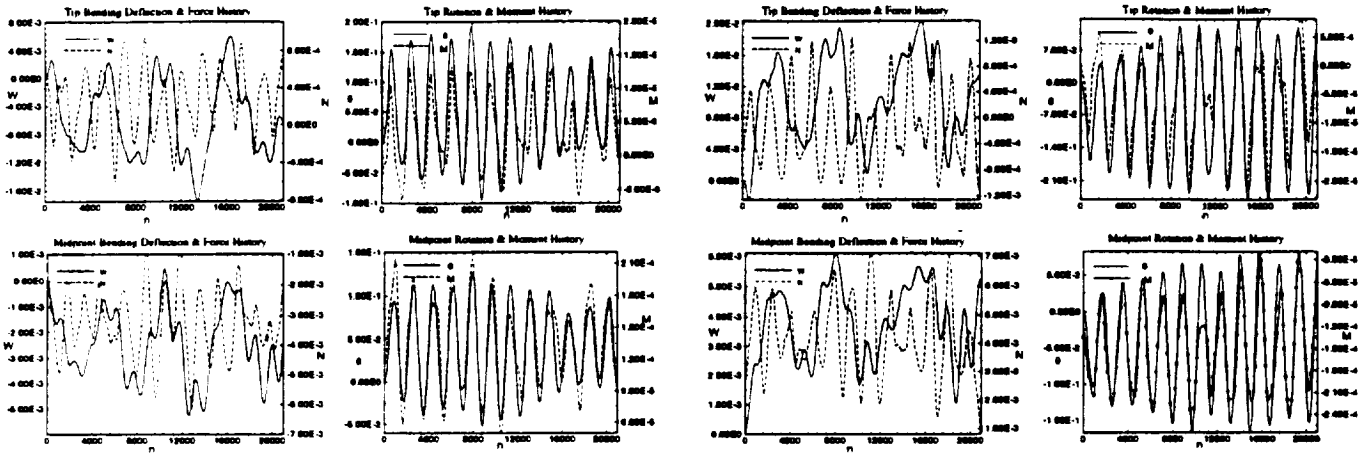

(a) Left tail (b) Right tail

Figure 5: History of the deflection and load responses for an uncoupled bending-torsion case. $M_\infty = 0.3$, $\alpha = 30^o$, $R_e = 1.25x10^6$, (Inboard position).

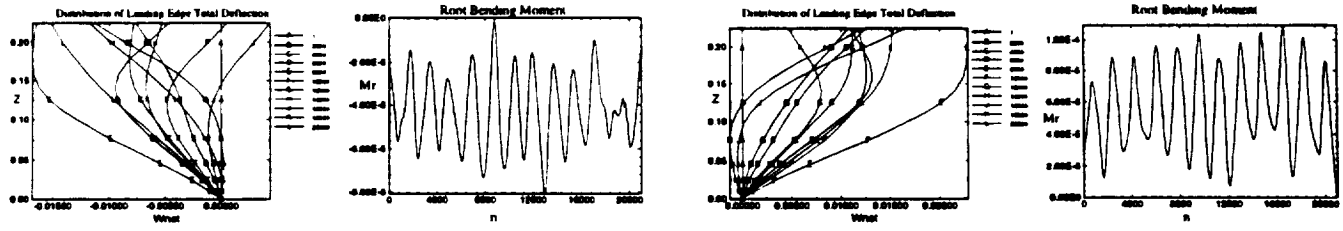

(a) Left tail (b) Right tail

Figure 6: Total structural deflections and root bending moment for an uncoupled bending-torsion case. $M_\infty = 0.3$, $\alpha = 30^o$, $R_e = 1.25x10^6$, (Inboard position).

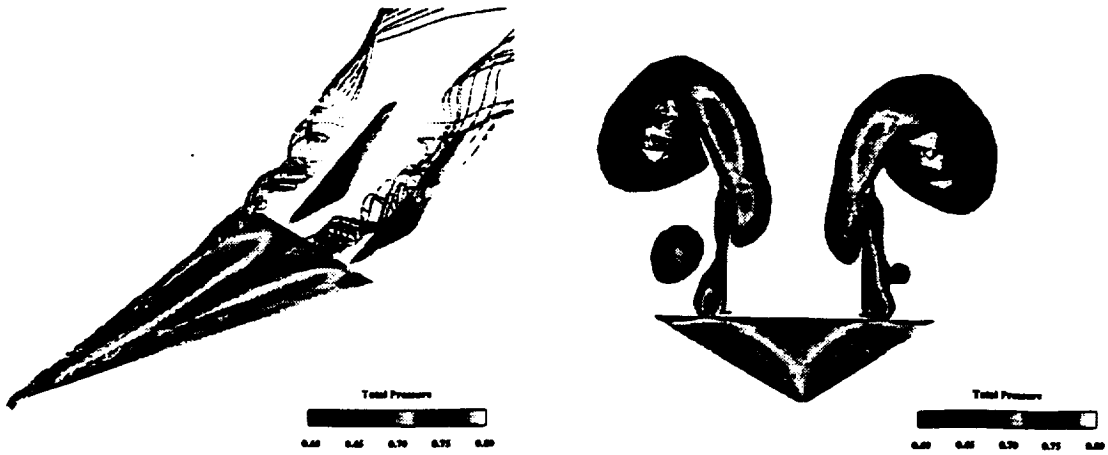

Figure 7: Three-dimensional and front views showing the total pressure on the surfaces, and the vortex-core streamlines. Uncoupled case after $it = 9,600$ (Midspan position).

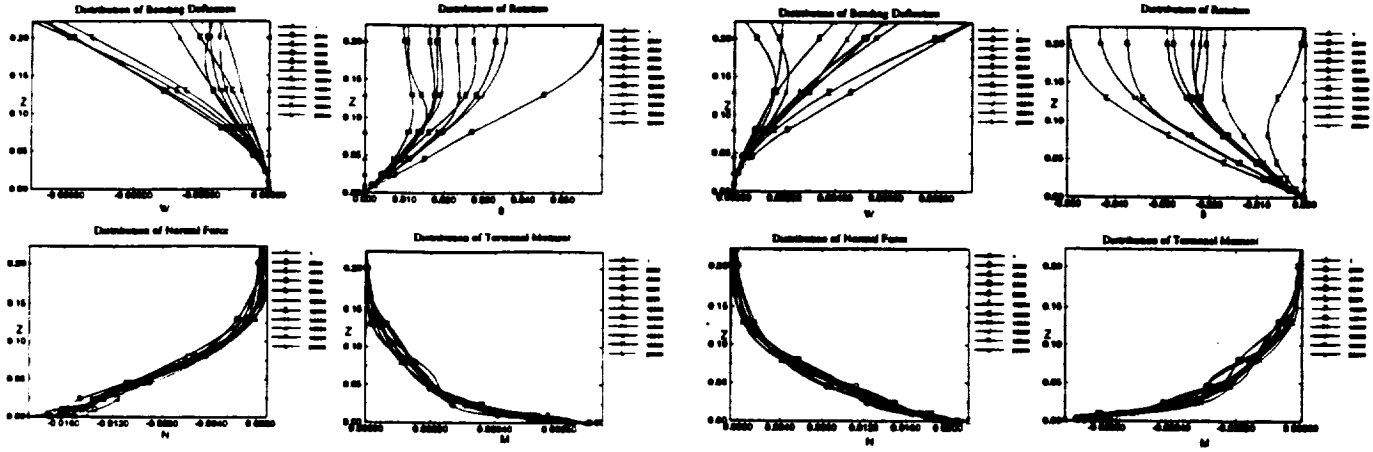

(a) Left tail (b) Right tail

Figure 8: Distribution of the deflection and load responses for an uncoupled bending-torsion case. $M_\infty = 0.3$, $\alpha = 30^o$, $R_e = 1.25x10^6$, (Midspan position).

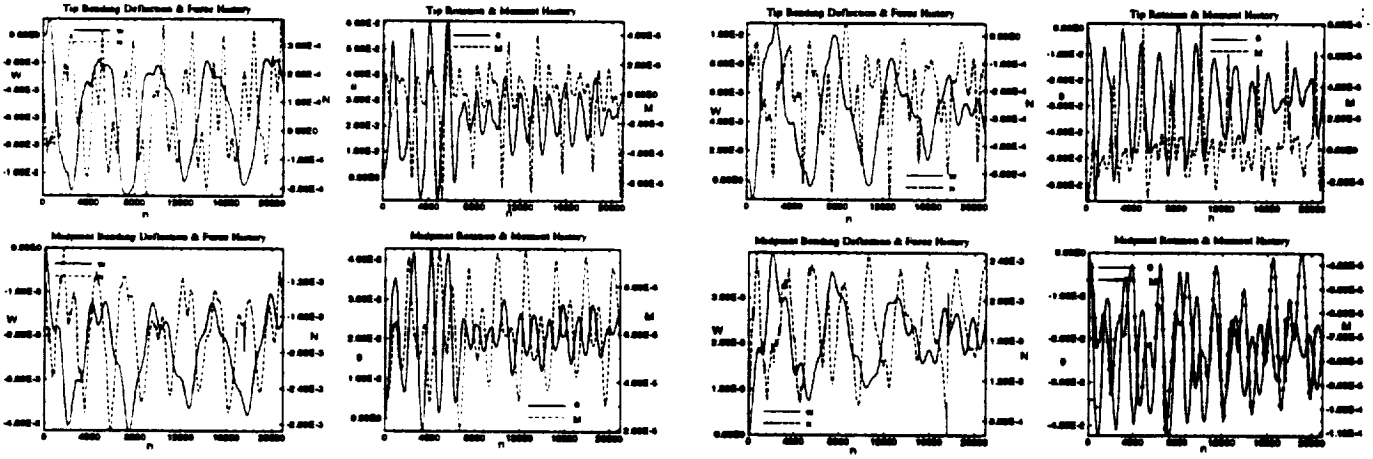

(a) Left tail (b) Right tail

Figure 9: History of the deflection and load responses for an uncoupled bending-torsion case. $M_\infty = 0.3$, $\alpha = 30^o$, $R_e = 1.25x10^6$, (Midspan position).

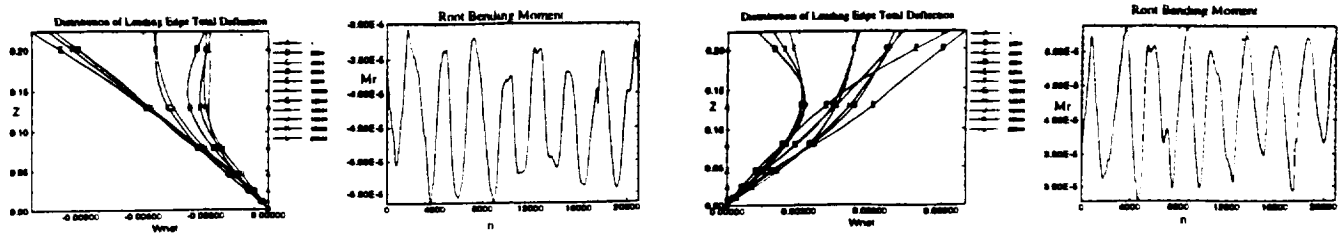

(a) Left tail (b) Right tail

Figure 10: Total structural deflections and root bending moment for an uncoupled bending-torsion case. $M_\infty = 0.3$, $\alpha = 30^o$, $R_e = 1.25x10^6$, (Midspan position).

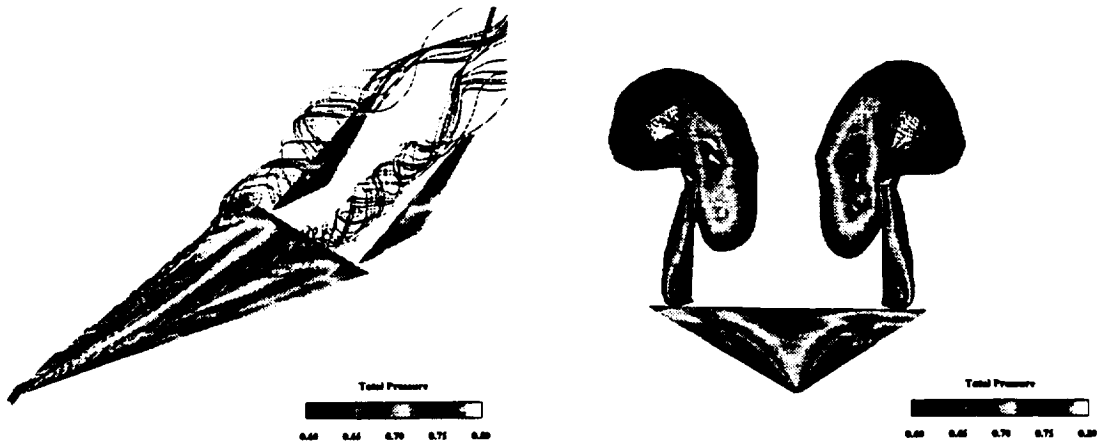

Figure 11: Three-dimensional and front views showing the total pressure on the surfaces, and the vortex-core streamlines. Uncoupled case after $it = 9,600$ (Outboard position).

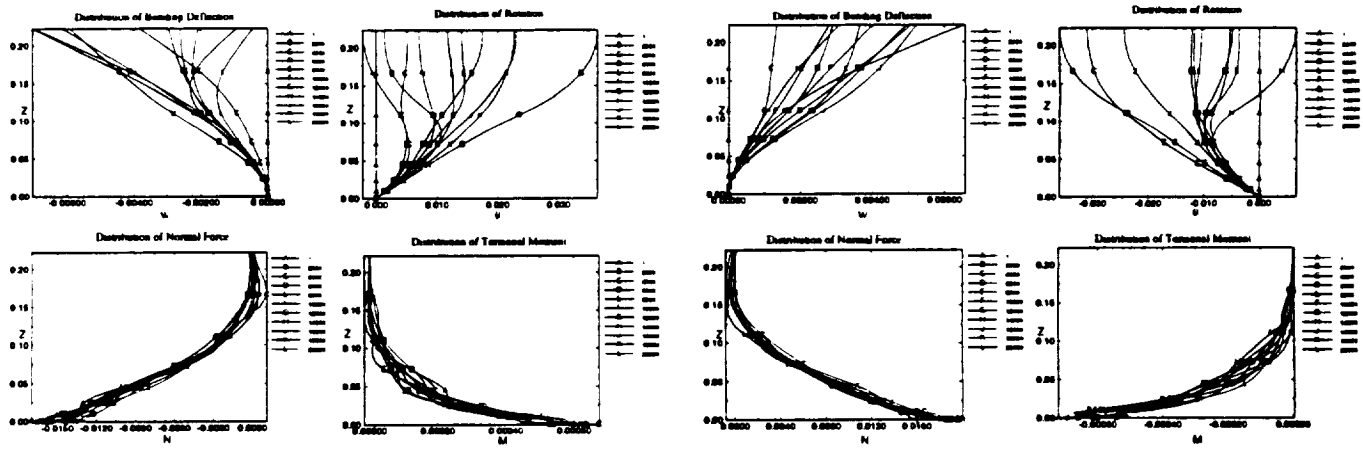

(a) Left tail (b) Right tail

Figure 12: Distribution of the deflection and load responses for an uncoupled bending-torsion case. $M_\infty = 0.3$, $\alpha = 30^o$, $R_e = 1.25x10^6$, (Outboard position).

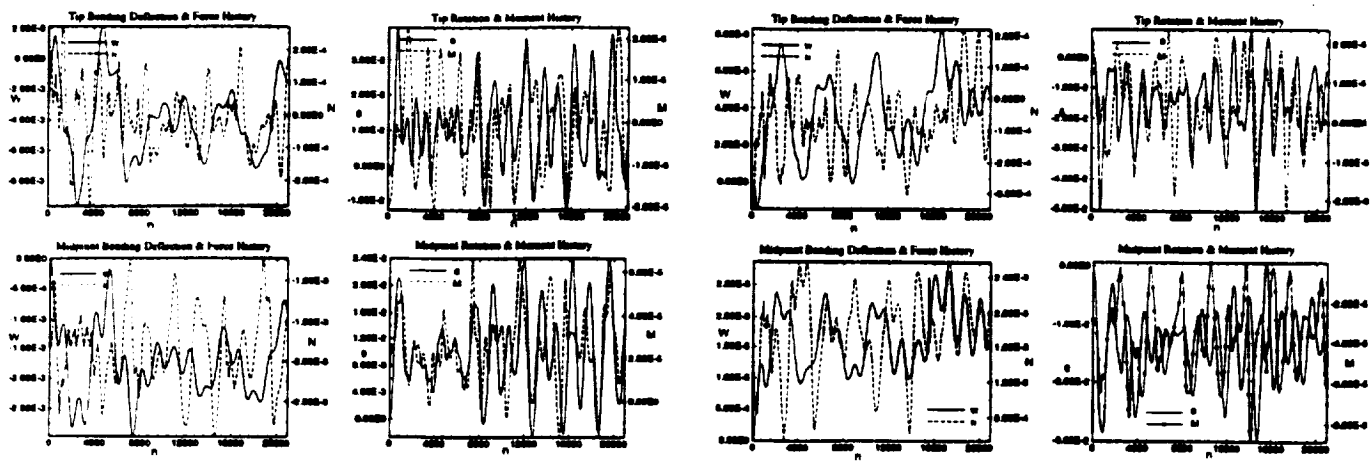

(a) Left tail (b) Right tail

Figure 13: History of the deflection and load responses for an uncoupled bending-torsion case. $M_\infty = 0.3$, $\alpha = 30^o$, $R_e = 1.25x10^6$, (Outboard position).

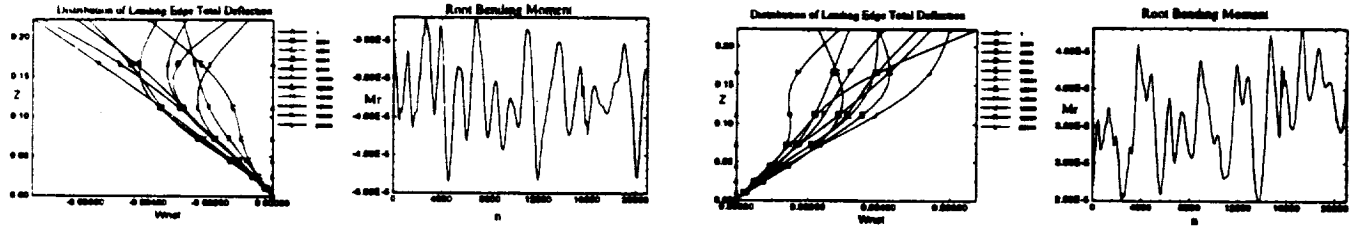

(a) Left tail (b) Right tail

Figure 14: Total structural deflections and root bending moment for an uncoupled bending-torsion case. $M_\infty = 0.3$, $\alpha = 30^o$, $R_e = 1.25x10^6$, (Outboard position).